Geophysical Prospecting **38**, 633–661, 1990

DECOMPOSITION OF MULTICOMPONENT SEISMIC DATA INTO PRIMARY P- AND S-WAVE RESPONSES[1]

C. P. A. WAPENAAR, P. HERRMANN, D. J. VERSCHUUR and A. J. BERKHOUT[2]

ABSTRACT

WAPENAAR, C.P.A., HERRMANN, P., VERSCHUUR, D.J. and BERKHOUT, A.J. 1990. Decomposition of multicomponent seismic data into primary P- and S-wave responses. *Geophysical Prospecting* **38**, 633–661.

Inversion of multicomponent seismic data can be subdivided in three main processes: (1) Surface-related preprocessing (decomposition of the multicomponent data into 'primary' P- and S-wave responses). (2) Prestack migration of the primary P- and S-wave responses, yielding the (angle-dependent) P–P, P–S, S–P and S–S reflectivity of the subsurface. (3) Target-related post-processing (transformation of the reflectivity into the rock and pore parameters in the target). This paper deals with the theoretical aspects of surface-related preprocessing.

In a multicomponent seismic data set the P- and S-wave responses of the subsurface are distorted by two main causes: (1) The seismic vibrators always radiate a mixture of P- and S-waves into the subsurface. Similarly, the geophones always measure a mixture of P- and S-waves. (2) The free surface reflects any upgoing wave fully back into the subsurface. This gives rise to strong multiple reflections, including conversions.

Therefore, surface-related preprocessing consists of two steps: (1) Decomposition of the multicomponent data (pseudo P- and S-wave responses) into true P- and S-wave responses. In practice this procedure involves (a) decomposition per common shot record of the particle velocity vector into scalar upgoing P- and S-waves, followed by (b) decomposition per common receiver record of the traction vector into scalar downgoing P- and S-waves. (2) Elimination of the surface-related multiple reflections and conversions. In this procedure the free surface is replaced by a reflection-free surface. The effect is that we obtain 'primary' P- and S-wave responses, that contain internal multiples only.

[1] Paper read at the 51st EAEG meeting, Berlin, May–June 1989; revision accepted February 1990.

[2] Delft University of Technology, Laboratory of Seismics and Acoustics, P.O. Box 5046, 2600 GA Delft, The Netherlands.

An interesting aspect of the procedure is that no knowledge of the subsurface is required. In fact, the subsurface may have any degree of complexity. Both the decomposition step and the multiple elimination step are fully determined by the medium parameters at the free surface only. After surface-related preprocessing, the scalar P- and S-wave responses can be further processed independently by existing scalar algorithms.

INTRODUCTION

In the seismic industry there is an important trend towards multicomponent data acquisition. Compared with conventional single-component data, multicomponent data contain much additional information about the elastic parameters of the subsurface. Of course, the key question is how to resolve this additional information in a sensible and economic way. Recently Berkhout and Wapenaar (1988) proposed a new elastic seismic processing scheme which contains a number of distinct modules (Fig. 1). Each module represents one seismic processing step (ranging from decomposition of the multicomponent data to lithologic inversion for rock and pore parameters) and is based on physical principles.

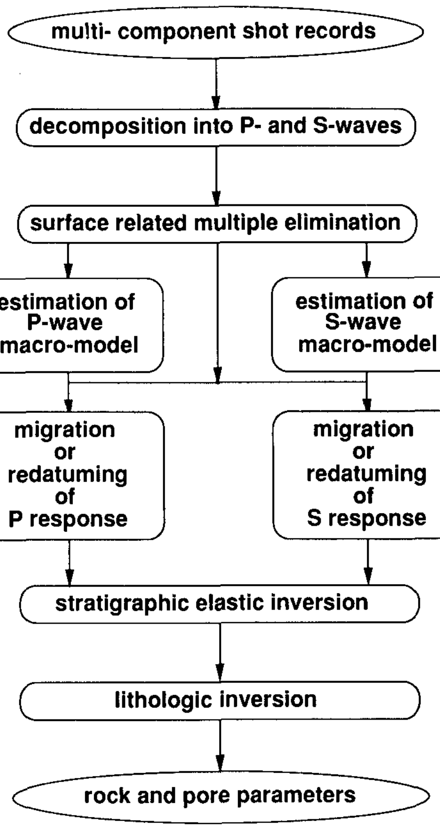

FIG. 1. Elastic seismic processing scheme, a stepwise approach.

This paper deals with the theoretical aspects of the following two surface-related preprocessing steps: (1) Decomposition into P- and S-wave responses. (2) Elimination of the surface-related multiples and conversions.

The main effect of these two steps is that the vector data at the free surface are transformed into a number of independent scalar responses at a reflection-free acquisition surface (compare Figs 12 and 15). These scalar responses can be further processed independently by scalar schemes such as prestack migration or redatuming. Any existing or future scheme can be used for this purpose. Preferably, the acoustic extrapolation operators should be replaced by elastic extrapolation operators for P- and/or S-waves (Wapenaar and Haimé 1990).

Historical Outline

Without claiming completeness, we give an outline of some highlights in the history of surface-related preprocessing. For horizontally-layered elastic media, Kennett (1979) derived a procedure for the elimination of surface-related multiples from 2D multicomponent seismic data. Berkhout (1982) published the first multiple elimination scheme which deals with *laterally varying* 2D acoustic media; recent examples may be found in Verschuur, Berkhout and Wapenaar (1989). Kennett (1984) extended Berkhout's scheme for the elastic situation. Both Berkhout and Kennett acknowledged that source and receiver effects must be removed from the data before the multiple elimination can be applied successfully. For the elastic situation removal of source and receiver effects means decomposition into downgoing and upgoing P- and S-waves. Dankbaar (1985) published a scheme for decomposing receiver data into upgoing P- and S-waves. We discuss a wave theoretical approach to decomposition of the source and receiver data into downgoing and upgoing P- and S-waves, followed by elimination of the surface-related multiple reflections and conversions. The theory is presented for arbitrarily inhomogeneous anisotropic 3D subsurface configurations. The surface layer may be inhomogeneous but it is assumed to be isotropic.

Forward Model of Multicomponent Seismic Data

Before we discuss the decomposition scheme we present a forward model of multicomponent seismic data. We show step by step that this forward model is obtained by applying a number of simple matrix manipulations to the primary P- and S-wave responses of the subsurface. An important consequence is that decomposition of multicomponent seismic data may be accomplished by applying the same matrix manipulations in reverse order.

First we consider the forward model of the primary response of an acoustic subsurface bounded by a reflection-free surface at z_0. With reference to Fig. 2a, we write

$$\mathbf{p}^-(z_0) = \mathbf{X}(z_0)\mathbf{p}^+(z_0), \tag{1}$$

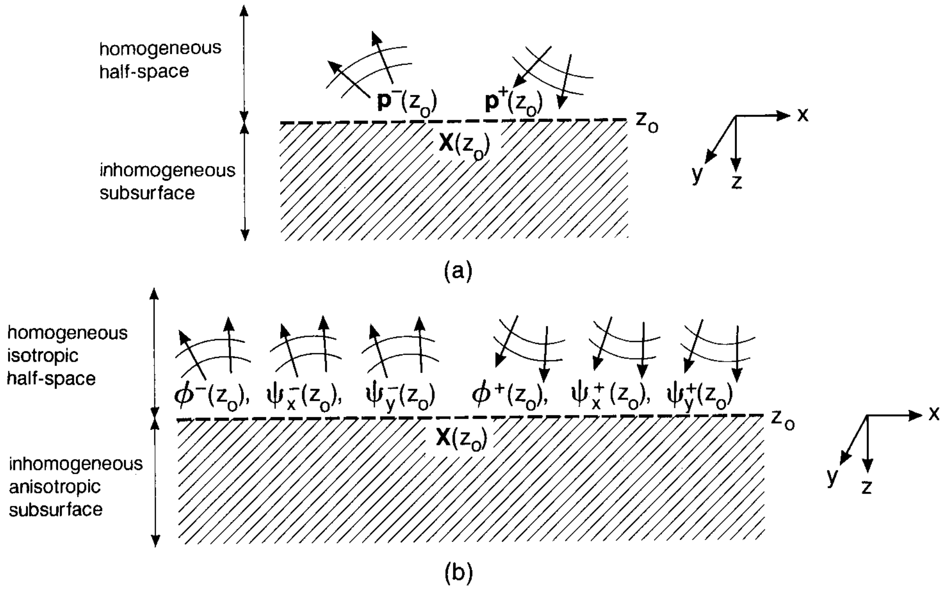

FIG. 2. The primary one-way response matrix $\mathbf{X}(z_0)$ describes the relationship between primary downgoing and upgoing wavefields at depth level z_0. (a) Acoustic version: vectors $\mathbf{p}^+(z_0)$ and $\mathbf{p}^-(z_0)$ represent the pressure of the downgoing and upgoing waves at z_0. (b) Elastic version: vectors $\boldsymbol{\phi}^+(z_0)$ and $\boldsymbol{\phi}^-(z_0)$ represent the potentials for the downgoing and upgoing compressional waves at z_0; vectors $\boldsymbol{\psi}_x^+(z_0)$, $\boldsymbol{\psi}_y^+(z_0)$ and $\boldsymbol{\psi}_x^-(z_0)$, $\boldsymbol{\psi}_y^-(z_0)$ represent the potentials for the downgoing and upgoing shear waves at z_0 (the subscripts x and y refer to the different polarizations).

(Berkhout 1982). Here vector $\mathbf{p}^+(z_0)$ represents a 3D monochromatic downgoing acoustic wavefield at depth level z_0 (the matrix/vector notation for discretized wavefields is explained in Appendix A). This acoustic wavefield propagates into the 3D inhomogeneous subsurface $z > z_0$, is partly reflected at the layer boundaries and propagates back to the surface. The 3D upgoing wavefield arriving at the surface z_0 is denoted by $\mathbf{p}^-(z_0)$. According to (1), the primary one-way response matrix $\mathbf{X}(z_0)$ describes the relationship between the downgoing and upgoing one-way wavefields at z_0. Here and in the following the adjective 'primary' refers to the absence of multiple reflections related to surface z_0; internal multiple reflections occurring in the 3D inhomogeneous subsurface are included in $\mathbf{X}(z_0)$.

Next we consider an elastic subsurface bounded by a reflection-free surface at z_0 (Fig. 2b). Again the forward model of the primary response is given by (1), where the wavefield vectors $\mathbf{p}^-(z_0)$ and $\mathbf{p}^+(z_0)$ each contain three sub-vectors, according to

$$\mathbf{p}^-(z_0) = \begin{pmatrix} \boldsymbol{\phi}^-(z_0) \\ \boldsymbol{\psi}_x^-(z_0) \\ \boldsymbol{\psi}_y^-(z_0) \end{pmatrix} \text{ and } \mathbf{p}^+(z_0) = \begin{pmatrix} \boldsymbol{\phi}^+(z_0) \\ \boldsymbol{\psi}_x^+(z_0) \\ \boldsymbol{\psi}_y^+(z_0) \end{pmatrix}, \tag{2a}$$

whereas the response matrix $\mathbf{X}(z_0)$ contains nine sub-matrices, according to

$$\mathbf{X}(z_0) = \begin{pmatrix} \mathbf{X}_{\phi,\phi}(z_0) & \mathbf{X}_{\phi,\psi_x}(z_0) & \mathbf{X}_{\phi,\psi_y}(z_0) \\ \mathbf{X}_{\psi_x,\phi}(z_0) & \mathbf{X}_{\psi_x,\psi_x}(z_0) & \mathbf{X}_{\psi_x,\psi_y}(z_0) \\ \mathbf{X}_{\psi_y,\phi}(z_0) & \mathbf{X}_{\psi_y,\psi_x}(z_0) & \mathbf{X}_{\psi_y,\psi_y}(z_0) \end{pmatrix}, \tag{2b}$$

(Wapenaar and Berkhout 1989). Vectors $\boldsymbol{\phi}^+(z_0)$ and $\boldsymbol{\phi}^-(z_0)$ represent the potentials for the 3D monochromatic downgoing and upgoing compressional (P) waves at depth level z_0; vectors $\boldsymbol{\psi}_x^+(z_0)$, $\boldsymbol{\psi}_y^+(z_0)$ and $\boldsymbol{\psi}_x^-(z_0)$, $\boldsymbol{\psi}_y^-(z_0)$ represent the potentials for the downgoing and upgoing shear (S_x, S_y) waves at z_0 (the sub-scripts x and y refer to the different polarizations, see also Appendix B). Any of the sub-matrices in (2b) represents a primary response of the elastic subsurface. For example, matrix $\mathbf{X}_{\phi,\psi_y}(z_0)$ describes the relationship between downgoing S_y waves (polarized in the plane perpendicular to the y-axis) and upgoing P- waves at z_0. The one-way forward model of (1) is visualized by the block-diagram of Fig. 3.

So far we have assumed that surface z_0 is reflection free. In practical seismic situations, however, surface z_0 represents the Earth's free surface which is a perfect reflector for the upgoing waves $\mathbf{p}^-(z_0)$. Therefore in the forward model of (1) we should write for the total downgoing wavefield at z_0

$$\mathbf{p}^+(z_0) = \mathbf{p}_r^+(z_0) + \mathbf{p}_s^+(z_0). \tag{3a}$$

Here vector $\mathbf{p}_r^+(z_0)$ is the downgoing reflected wavefield at z_0, according to

$$\mathbf{p}_r^+(z_0) = \mathbf{R}_{fr}^-(z_0)\mathbf{p}^-(z_0), \tag{3b}$$

where matrix $\mathbf{R}_{fr}^-(z_0)$ describes the reflectivity (including conversion) of the Earth's free surface for upgoing waves. For an acoustic free surface we may simply write

$$\mathbf{R}_{fr}^-(z_0) = -\mathbf{I}, \tag{3c}$$

where $\mathbf{I}$ is the identity matrix. For an elastic free surface $\mathbf{R}_{fr}^-(z_0)$ is derived in Appendix B (B20). In (3a), vector $\mathbf{p}_s^+(z_0)$ contains the downgoing source wavefields at z_0. The relationship between $\mathbf{p}_s^+(z_0)$ and the seismic sources at z_0 is discussed later. Upon substitution of (3a) and (3b) into the forward model (1) we obtain the following implicit expression for the upgoing wavefield at z_0:

$$\mathbf{p}^-(z_0) = \mathbf{X}(z_0)[\mathbf{R}_{fr}^-(z_0)\mathbf{p}^-(z_0) + \mathbf{p}_s^+(z_0)], \tag{4}$$

see Fig. 4. This expression can be rewritten explicitly, according to

$$\mathbf{p}^-(z_0) = \mathbf{X}_{fr}(z_0)\mathbf{p}_s^+(z_0), \tag{5a}$$

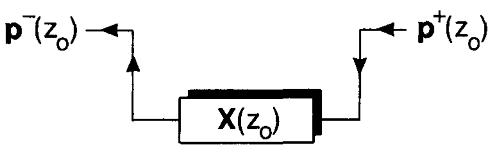

FIG. 3. One-way forward model of the primary response of an acoustic or elastic subsurface, bounded by a reflection free surface at z_0.

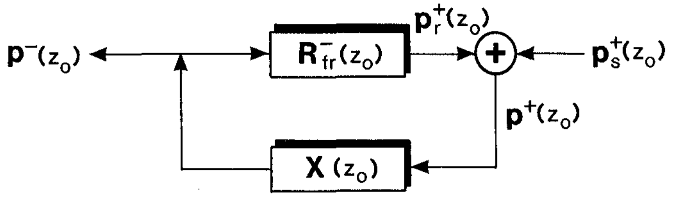

FIG. 4. One-way forward model, including surface-related multiple reflections and conversions.

where the free surface one-way response matrix $\mathbf{X}_{fr}(z_0)$ is defined as

$$\mathbf{X}_{fr}(z_0) = [\mathbf{I} - \mathbf{X}(z_0)\mathbf{R}^-_{fr}(z_0)]^{-1}\mathbf{X}(z_0), \tag{5b}$$

or, rewriting the inverse matrix as a series expansion,

$$\mathbf{X}_{fr}(z_0) = \left[\mathbf{I} + \sum_{m=1}^{\infty} (\mathbf{X}(z_0)\mathbf{R}^-_{fr}(z_0))^m\right]\mathbf{X}(z_0). \tag{5c}$$

The latter expression clearly shows that the free surface generates an infinite number of multiple reflections and conversions.

Next we discuss the relationship between the one-way wavefields in the forward model (5) and the two-way seismic data. According to (B18a), the general relationship between two-way and one-way elastic wavefields reads

$$\begin{pmatrix} \mathbf{v}(z) \\ \boldsymbol{\tau}(z) \end{pmatrix} = \begin{pmatrix} \mathbf{L}^+_1(z) & \mathbf{L}^-_1(z) \\ \mathbf{L}^+_2(z) & \mathbf{L}^-_2(z) \end{pmatrix} \begin{pmatrix} \mathbf{p}^+(z) \\ \mathbf{p}^-(z) \end{pmatrix}, \tag{6a}$$

where the three-component velocity and traction vectors $\mathbf{v}(z)$ and $\boldsymbol{\tau}(z)$ are defined according to

$$\mathbf{v}(z) = \begin{pmatrix} \mathbf{v}_x(z) \\ \mathbf{v}_y(z) \\ \mathbf{v}_z(z) \end{pmatrix} \text{ and } \boldsymbol{\tau}(z) = \begin{pmatrix} \boldsymbol{\tau}_x(z) \\ \boldsymbol{\tau}_y(z) \\ \boldsymbol{\tau}_z(z) \end{pmatrix}, \tag{6b}$$

matrices $\mathbf{L}^{\pm}_{\alpha}(z)$ for $\alpha = 1, 2$ are defined by (B18b) and vectors $\mathbf{p}^{\pm}(z)$ are defined as in (2a). In (6b), vectors $\mathbf{v}_x(z)$, $\mathbf{v}_y(z)$ and $\mathbf{v}_z(z)$ represent the velocity components of the 3D elastic wavefield at depth level z; vectors $\boldsymbol{\tau}_x(z)$, $\boldsymbol{\tau}_y(z)$ and $\boldsymbol{\tau}_z(z)$ represent the traction components of the same wavefield at depth level z.

In the following we restrict ourselves for simplicity to the situation where the sources and receivers are at the free surface (Fig. 5). We define a source-decomposition operator $\mathbf{D}(z_0)$ which describes the relationship between the traction source vector $\boldsymbol{\tau}_s(z_0)$ at the free surface and the downgoing source wave vector $\mathbf{p}^+_s(z_0)$, according to

$$\mathbf{p}^+_s(z_0) \triangleq \mathbf{D}(z_0)\boldsymbol{\tau}_s(z_0). \tag{7a}$$

On the other hand, since the upgoing source wavefields at z_0 must be zero, we derive from (6a)

$$\boldsymbol{\tau}_s(z_0) = \mathbf{L}^+_2(z_0)\mathbf{p}^+_s(z_0) + \mathbf{0}. \tag{7b}$$

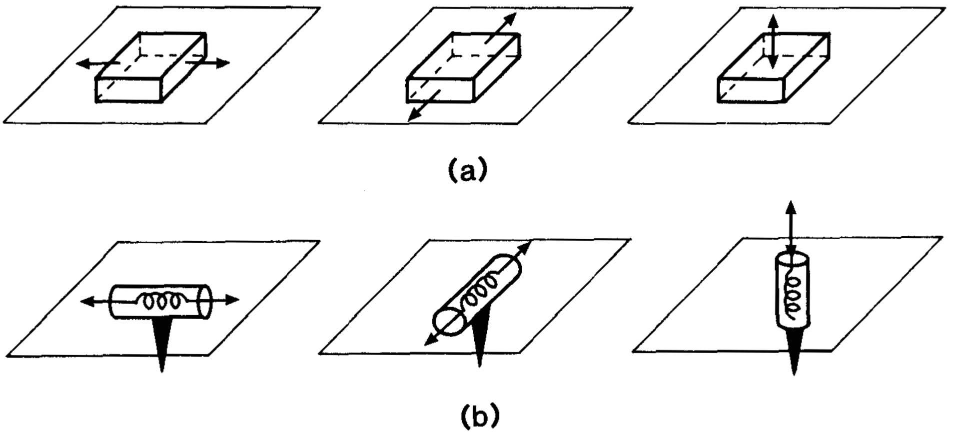

FIG. 5. Multicomponent data acquisition. (a) Three differently oriented seismic vibrators, imposing stresses in the x-, y- and z-direction to the earth's surface. (b) Three differently oriented geophones, measuring the x-, y- and z-components of the particle velocity at the earth's surface.

Hence, the source-decomposition operator reads

$$\mathbf{D}(z_0) = [\mathbf{L}_2^+(z_0)]^{-1}. \tag{7c}$$

Next we derive an expression for the receiver-composition operator $\mathbf{C}(z_0)$. For velocity receivers at the free surface (geophones, see Fig. 5b) we derive from (6a) and (3a)

$$\mathbf{v}(z_0) = \mathbf{L}_1^+(z_0)(\mathbf{p}_r^+(z_0) + \mathbf{p}_s^+(z_0)) + \mathbf{L}_1^-(z_0)\mathbf{p}^-(z_0), \tag{8a}$$

or, ignoring the contribution of the direct source wave $\mathbf{p}_s^+(z_0)$ and substituting (3b) for the reflected waves $\mathbf{p}_r^+(z_0)$

$$\mathbf{v}(z_0) = \mathbf{L}_1^+(z_0)\mathbf{R}_{fr}^-(z_0)\mathbf{p}^-(z_0) + \mathbf{L}_1^-(z_0)\mathbf{p}^-(z_0), \tag{8b}$$

or, upon substitution of (B20c) for the free surface reflection matrix $\mathbf{R}_{fr}^-(z_0)$,

$$\mathbf{v}(z_0) = [-\mathbf{L}_1^+(z_0)(\mathbf{L}_2^+(z_0))^{-1}\mathbf{L}_2^-(z_0) + \mathbf{L}_1^-(z_0)]\mathbf{p}^-(z_0). \tag{8c}$$

Hence, if we define the receiver-composition process as

$$\mathbf{v}(z_0) \triangleq \mathbf{C}(z_0)\mathbf{p}^-(z_0), \tag{9a}$$

then the receiver-composition operator reads

$$\mathbf{C}(z_0) = -\mathbf{L}_1^+(z_0)(\mathbf{L}_2^+(z_0))^{-1}\mathbf{L}_2^-(z_0) + \mathbf{L}_1^-(z_0), \tag{9b}$$

or, according to (B19a)

$$\mathbf{C}(z_0) = [\mathbf{M}_1^-(z_0)]^{-1}, \tag{9c}$$

with $\mathbf{M}_1^-(z_0)$ defined by (B17e). Note that the one-way forward model (5a) may be elegantly combined with the decomposition and composition algorithms (7a) and

(9a), yielding

$$\mathbf{v}(z_0) = \mathbf{C}(z_0)\mathbf{X}_{\mathrm{fr}}(z_0)\mathbf{D}(z_0)\boldsymbol{\tau}_{\mathrm{s}}(z_0), \tag{10a}$$

where

$$\mathbf{X}_{\mathrm{fr}}(z_0) = [\mathbf{I} - \mathbf{X}(z_0)\mathbf{R}^-_{\mathrm{fr}}(z_0)]^{-1}\mathbf{X}(z_0), \tag{10b}$$

see also Fig. 6. From right to left (10a) contains a source vector (describing the stress distribution of a seismic vibrator at the free surface), a decomposition matrix (transforming the traction into downgoing P- and S-waves), a one-way response matrix (describing the response of the subsurface, including multiple reflections and conversions related to the free surface), and a composition matrix (transforming the upgoing P- and S-waves into velocities at the free surface). It may be concluded that (10) is the forward model of one (monochromatic) multicomponent shot record, ignoring direct waves. In accordance with (6b), vector $\mathbf{v}(z_0)$ contains the velocity components measured by the geophones at the free surface. Also in accordance with (6b), vector $\boldsymbol{\tau}_{\mathrm{s}}(z_0)$ contains the vectors $\boldsymbol{\tau}_{x,\mathrm{s}}(z_0)$, $\boldsymbol{\tau}_{y,\mathrm{s}}(z_0)$ and $\boldsymbol{\tau}_{z,\mathrm{s}}(z_0)$. For a point source of tensile stress (a vertical vibrator), vector $\boldsymbol{\tau}_{z,\mathrm{s}}(z_0)$ contains only one non-zero element, its value representing the source signature $s(\omega)$. Similarly, for a point source of shearing stress (a horizontal vibrator), one of the vectors $\boldsymbol{\tau}_{x,\mathrm{s}}(z_0)$ or $\boldsymbol{\tau}_{y,\mathrm{s}}(z_0)$ contains only one non-zero element, its value representing $s(\omega)$. When the vibrators are not ideal point sources as in Fig. 5a, then the source vector contains the stress distribution at z_0. The forward model for one shot record can be extended easily to a forward model for a complete seismic survey. Ideally, in the elastic situation three independent seismic experiments should be carried out for each source position by applying three differently oriented seismic vibrators. For a 3×3 component seismic survey the extended forward model reads

$$\mathbf{V}(z_0) = \mathbf{C}(z_0)\mathbf{X}_{\mathrm{fr}}(z_0)\mathbf{D}(z_0)\mathbf{T}_{\mathrm{s}}(z_0). \tag{11a}$$

Here the columns of the data matrix $\mathbf{V}(z_0)$ contain the different data vectors $\mathbf{v}(z_0)$. The columns of the source matrix $\mathbf{T}_{\mathrm{s}}(z_0)$ contain the corresponding source vectors $\boldsymbol{\tau}_{\mathrm{s}}(z_0)$. When use is made of independent horizontal vibrators and vertical vibrators (Fig. 5a), then the source vectors can be ordered in such a way that the source

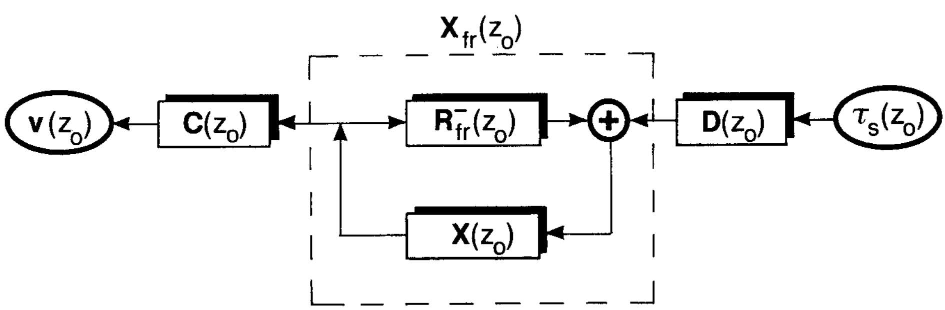

FIG. 6. Forward model for multicomponent seismic data (the direct waves are ignored).

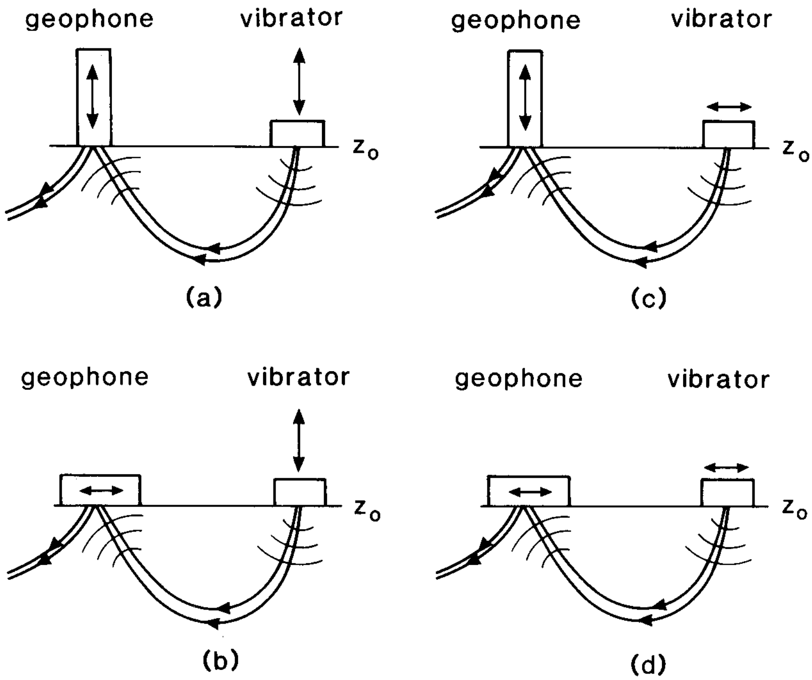

FIG. 7. 2D visualization of multicomponent data acquisition at a free surface z_0. The double raypaths represent P- and S-waves.

matrix can be written as

$$\mathbf{T}_s(z_0) = \begin{pmatrix} \mathbf{T}_{x,s}(z_0) & \mathbf{0} & \mathbf{0} \\ \mathbf{0} & \mathbf{T}_{y,s}(z_0) & \mathbf{0} \\ \mathbf{0} & \mathbf{0} & \mathbf{T}_{z,s}(z_0) \end{pmatrix}. \tag{11b}$$

Moreover, for identical point sources this expression may be further simplified to

$$\mathbf{T}_s(z_0) = s(\omega)\mathbf{I}. \tag{11c}$$

Now (11a) may be replaced by

$$\mathbf{V}(z_0) = \mathbf{C}(z_0)\mathbf{X}_{\mathrm{fr}}^{(s)}(z_0)\mathbf{D}(z_0), \tag{12a}$$

with

$$\mathbf{X}_{\mathrm{fr}}^{(s)}(z_0) = s(\omega)\mathbf{X}_{\mathrm{fr}}(z_0), \tag{12b}$$

and

$$\mathbf{V}(z_0) = \begin{pmatrix} \mathbf{V}_{x,x}(z_0) & \mathbf{V}_{x,y}(z_0) & \mathbf{V}_{x,z}(z_0) \\ \mathbf{V}_{y,x}(z_0) & \mathbf{V}_{y,y}(z_0) & \mathbf{V}_{y,z}(z_0) \\ \mathbf{V}_{z,x}(z_0) & \mathbf{V}_{z,y}(z_0) & \mathbf{V}_{z,z}(z_0) \end{pmatrix}. \tag{12c}$$

Here any of the sub-matrices $\mathbf{V}_{i,j}(z_0)$ for $i = x, y, z$ and $j = x, y, z$ represents a (monochromatic) single-component seismic survey, carried out with geophones oriented in the i-direction and vibrators oriented in the j-direction. In Fig. 7a the situation is shown for one element of matrix $\mathbf{V}_{z,z}(z_0)$. Similarly, in Figs 7b, c and d the situation is shown for the corresponding elements in matrices $\mathbf{V}_{x,z}(z_0)$, $\mathbf{V}_{z,x}(z_0)$ and $\mathbf{V}_{x,x}(z_0)$, respectively.

Finally we remark that the forward model we described is not a proposal for a numerical modelling scheme for multicomponent seismic data (we did not discuss the relationship between the subsurface parameters and the one-way response matrix and we ignored the direct waves). The only purpose of this section was to provide a starting point for a systematic discussion of the surface-related preprocessing scheme.

Decomposition into P- and S-Waves

Assume that a 3×3 component seismic survey has been carried out. When the different vibrators are oriented in arbitrary directions, then mutually perpendicular vibrators should be simulated by applying a weighted summation of the different responses. A similar remark can be made for the geophones (Cliet and Dubesset 1987). Before the decomposition can be carried out, the direct waves should be removed from the data. We do not discuss this procedure; a good reference is Beresford-Smith and Rango (1989). By applying a Fourier transform to each trace, the data are decomposed into monochromatic seismic surveys. Any of these monochromatic surveys satisfies the forward model described in the previous section. Our starting point for the discussion of the elastic decomposition scheme is (12), which is the forward model of a monochromatic multi-experiment multi-offset multicomponent seismic data set, excluding the direct waves. Assuming that the source signature $s(\omega)$ is unknown, the scaled free surface one-way response matrix can be obtained from the seismic data $\mathbf{V}(z_0)$ by inverting (12a), yielding

$$\mathbf{X}_{\mathrm{fr}}^{(s)}(z_0) = [\mathbf{C}(z_0)]^{-1}\mathbf{V}(z_0)[\mathbf{D}(z_0)]^{-1}, \tag{13a}$$

where

$$[\mathbf{D}(z_0)]^{-1} = \mathbf{L}_2^{+}(z_0) \tag{13b}$$

and

$$[\mathbf{C}(z_0)]^{-1} = \mathbf{M}_1^{-}(z_0), \tag{13c}$$

matrices $\mathbf{L}_2^{+}(z_0)$ and $\mathbf{M}_1^{-}(z_0)$ being defined by (B18b) and (B17e), respectively. Hence, decomposition of the two-way seismic data into one-way P- and S-wave responses may be carried out by applying the matrix operators $[\mathbf{C}(z_0)]^{-1}$ and $[\mathbf{D}(z_0)]^{-1}$ to the data matrix $\mathbf{V}(z_0)$, see Fig. 8. Note that $[\mathbf{C}(z_0)]^{-1}\mathbf{V}(z_0)$ describes a lateral deconvolution process along the columns (i.e., the monochromatic common shot records) of matrix $\mathbf{V}(z_0)$. This accounts for the decomposition of the received wavefields into upgoing P- and S-waves. Similarly, $\mathbf{V}(z_0)[\mathbf{D}(z_0)]^{-1}$ describes a lateral deconvolution process along the rows (i.e. the monochromatic common receiver records) of matrix

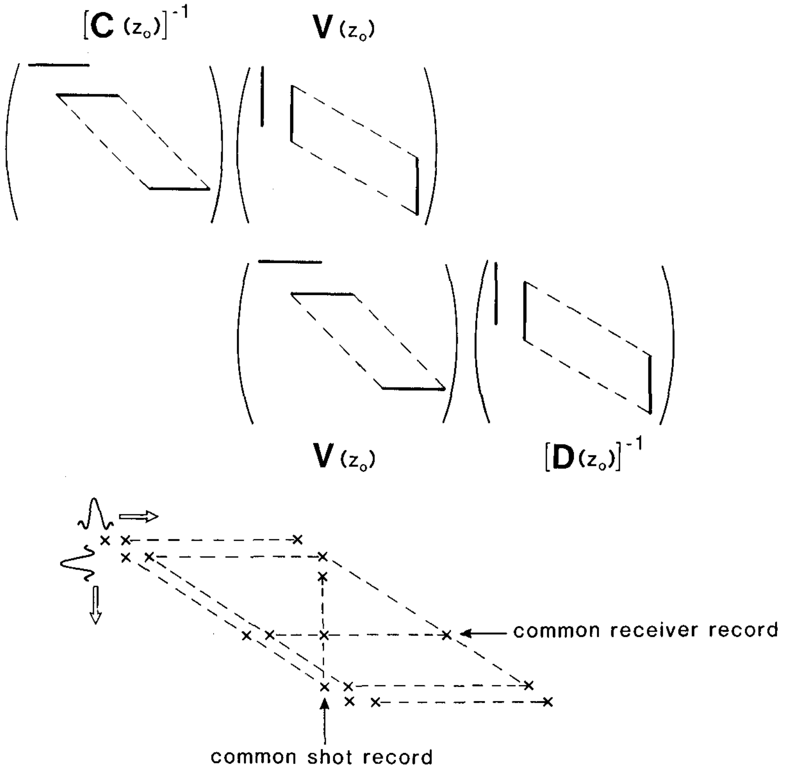

FIG. 8. According to (13), decomposition into P- and S-wave responses involves lateral deconvolution processes along the receivers in each common shot record and along the sources in each common receiver record. The same principle holds for prestack inverse wavefield extrapolation, as applied in depth migration.

$\mathbf{V}(z_0)$. This accounts for the decomposition of the emitted wavefields into downgoing P- and S-waves. Note the important similarity of (13a) with Berkhout's formulation for prestack inverse wavefield extrapolation, which is the nucleus of prestack migration (Berkhout 1982). Hence, the practical implementation of a decomposition scheme is very similar to the practical implementation of a prestack migration scheme. Like prestack migration, decomposition as formulated by (13) fully accounts for lateral variations of the medium parameters.

In analogy with (2b), the decomposed data matrix $\mathbf{X}_{\text{fr}}^{(s)}(z_0)$ may be written as

$$\mathbf{X}_{\text{fr}}^{(s)}(z_0) = \begin{pmatrix} \mathbf{X}_{\phi,\phi}(z_0) & \mathbf{X}_{\phi,\psi_x}(z_0) & \mathbf{X}_{\phi,\psi_y}(z_0) \\ \mathbf{X}_{\psi_x,\phi}(z_0) & \mathbf{X}_{\psi_x,\psi_x}(z_0) & \mathbf{X}_{\psi_x,\psi_y}(z_0) \\ \mathbf{X}_{\psi_y,\phi}(z_0) & \mathbf{X}_{\psi_y,\psi_x}(z_0) & \mathbf{X}_{\psi_y,\psi_y}(z_0) \end{pmatrix}_{\text{fr}}^{(s)}. \tag{14}$$

Any of the sub-matrices simulates a (monochromatic) single-component one-way seismic survey at the free surface. Matrices $(\mathbf{X}_{\phi,\phi}(z_0))_{\text{fr}}^{(s)}$ and $(\mathbf{X}_{\phi,\psi_\alpha}(z_0))_{\text{fr}}^{(s)}$ for $\alpha = x, y$ represent seismic surveys in terms of received upgoing P-waves related to sources in

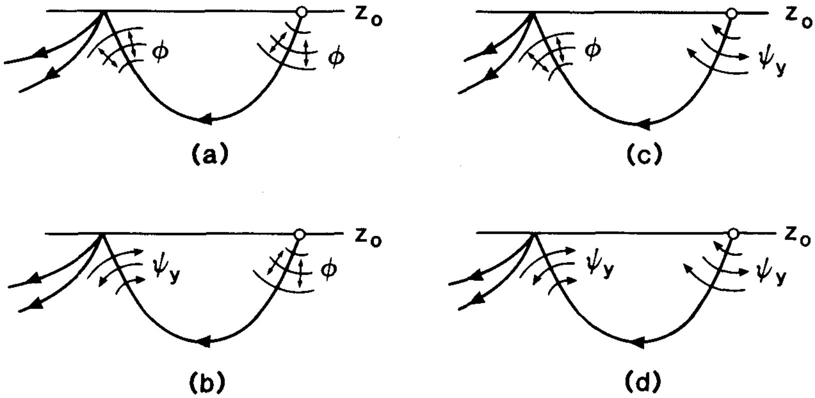

FIG. 9. 2D visualization of decomposed data at a free surface z_0.

terms of downgoing P-waves or downgoing S_x- or S_y-waves. Similarly, matrices $(\mathbf{X}_{\psi_\beta,\phi}(z_0))^{(s)}_{\mathrm{fr}}$ and $(\mathbf{X}_{\psi_\beta,\psi_\alpha}(z_0))^{(s)}_{\mathrm{fr}}$ for $\beta = x, y$ and $\alpha = x, y$ represent seismic surveys in terms of received upgoing S_x- or S_y-waves related to sources in terms of downgoing P-waves or downgoing S_x- or S_y-waves. In Fig. 9a the situation is shown for one element of matrix $(\mathbf{X}_{\phi,\phi}(z_0))^{(s)}_{\mathrm{fr}}$. Similarly, in Figs 9b, c and d the situation is shown for the corresponding elements in matrices $(\mathbf{X}_{\psi_y,\phi}(z_0))^{(s)}_{\mathrm{fr}}$, $(\mathbf{X}_{\phi,\psi_y}(z_0))^{(s)}_{\mathrm{fr}}$ and $(\mathbf{X}_{\psi_y,\psi_y}(z_0))^{(s)}_{\mathrm{fr}}$, respectively.

We illustrate the elastic decomposition procedure with a 2D example. For the subsurface configuration shown in Fig. 10, we generated 128 multicomponent seismic shot records by finite-difference modelling (Kelly *et al.* 1976; Haimé 1987). We used vertical and horizontal vibrators as well as vertical and horizontal geophones at the free surface z_0. One multicomponent shot record is shown in the space-time domain in Fig. 11. Figure 12 shows the same multicomponent shot record after removal of the ground roll. All multicomponent shot records are transformed from the time domain to the frequency domain, yielding a data matrix $\mathbf{V}(z_0)$

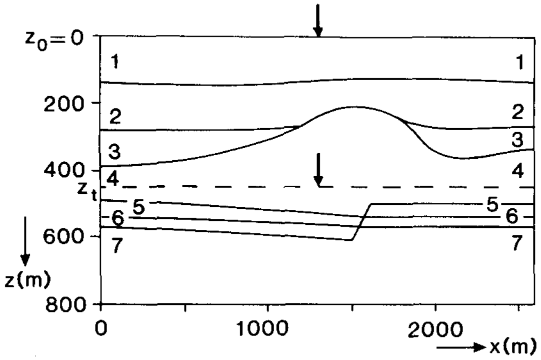

Layer	Cp(m/s)	Cs(m/s)	ρ(kg/m³)
1	2400	1400	1000
2	3000	2000	1600
3	3000	2000	2100
4	4100	2200	2200
5	3700	2000	2300
6	4200	2400	2000
7	3500	2100	1800

FIG. 10. 2D inhomogeneous elastic subsurface. The multicomponent vibrators and geophones are situated at the free surface $z_0 = 0$ m.

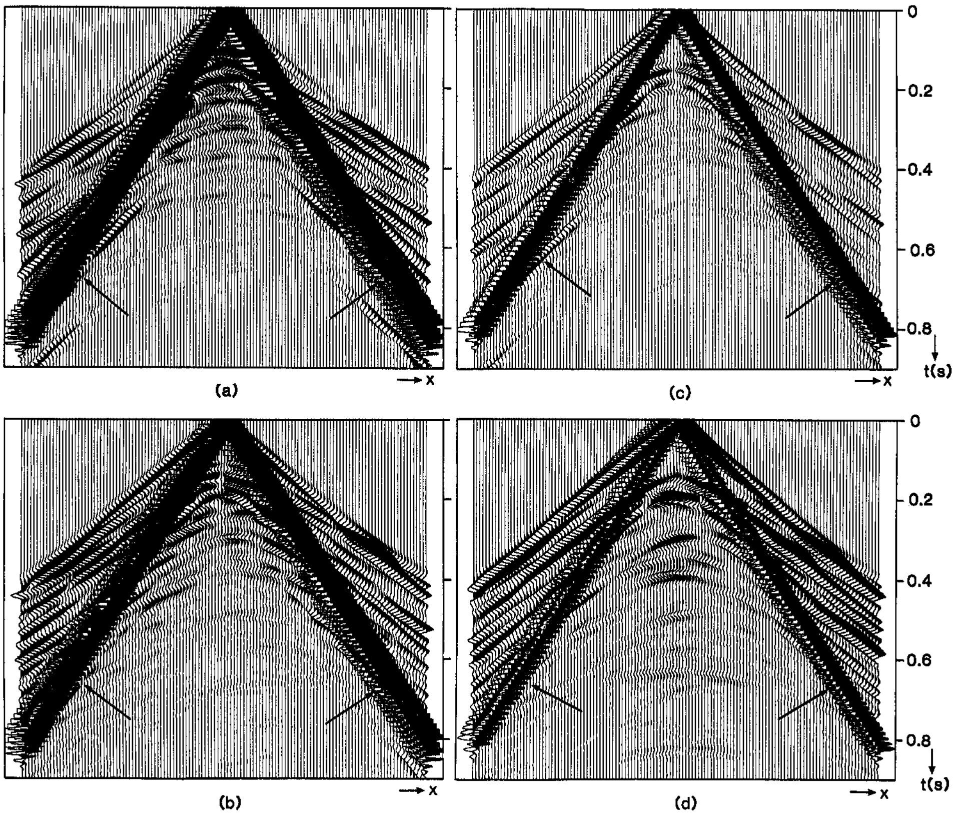

FIG. 11. Multicomponent shot record. The source position is indicated by the arrow in Fig. 10. (a) pseudo P–P data ($\mathbf{V}_{z,z}$, see Fig. 7a); (b) pseudo S_y–P data ($\mathbf{V}_{x,z}$, see Fig. 7b); (c) pseudo P–S_y data ($\mathbf{V}_{z,x}$, see Fig. 7c); (d) pseudo S_y–S_y data ($\mathbf{V}_{x,x}$, see Fig. 7d). The arrows indicate the ground roll.

for each frequency in the seismic band (5 Hz $< f = \omega/(2\pi) <$ 80 Hz). Next, decomposition is carried out by applying (13a) for each frequency in the seismic band. Finally, the results are transformed back from the frequency domain to the time domain. Figure 13 shows one multicomponent shot record after decomposition. Note that the spurious events, indicated by the arrows in Fig. 12, have vanished completely.

Elimination of Surface-Related Multiple Reflections and Conversions

After the decomposition has been carried out, the scaled multicomponent free surface one-way response matrix $\mathbf{X}_{\text{fr}}^{(s)}(z_0)$ is available for all frequencies in the seismic band. This response matrix contains significant multiple reflections and conversions related to the free surface (see Fig. 13). They can be removed by inverting (12b) and

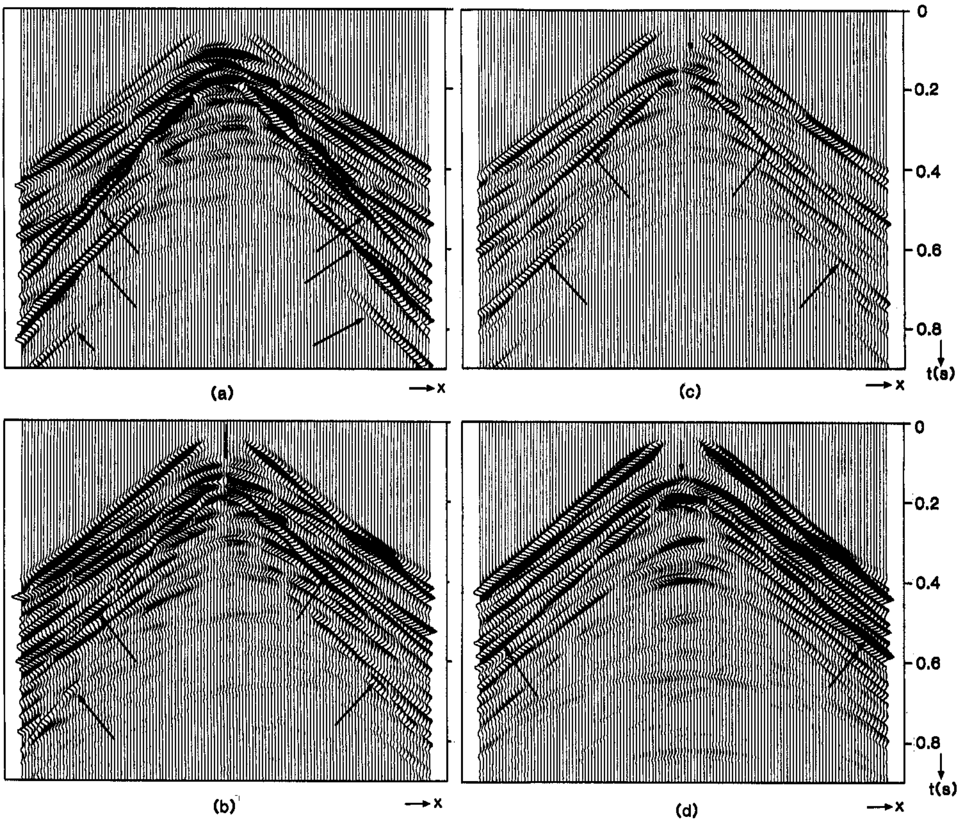

FIG. 12. Multicomponent shot record of Fig. 11 after removal of the ground roll: (a) pseudo P–P data; (b) pseudo S_y–P data; (c) pseudo P–S_y data; (d) pseudo S_y–S_y data. The arrows indicate spurious events.

(10b), yielding

$$\mathbf{X}_{\mathrm{fr}}(z_0) = \frac{1}{s(\omega)} \mathbf{X}_{\mathrm{fr}}^{(s)}(z_0), \tag{15a}$$

followed by

$$\mathbf{X}(z_0) = \mathbf{X}_{\mathrm{fr}}(z_0)[\mathbf{I} + \mathbf{R}_{\mathrm{fr}}^{-}(z_0)\mathbf{X}_{\mathrm{fr}}(z_0)]^{-1}, \tag{15b}$$

or, rewriting the inverse matrix as a series expansion,

$$\mathbf{X}(z_0) = \mathbf{X}_{\mathrm{fr}}(z_0)\left[\mathbf{I} + \sum_{m=1}^{\infty} (-\mathbf{R}_{\mathrm{fr}}^{-}(z_0)\mathbf{X}_{\mathrm{fr}}(z_0))^m\right]. \tag{15c}$$

Note that this 3D elastic multiple elimination scheme is identical to Berkhout's 2D acoustic multiple elimination scheme. The matrices in (15), though, are generalized versions of Berkhout's matrices.

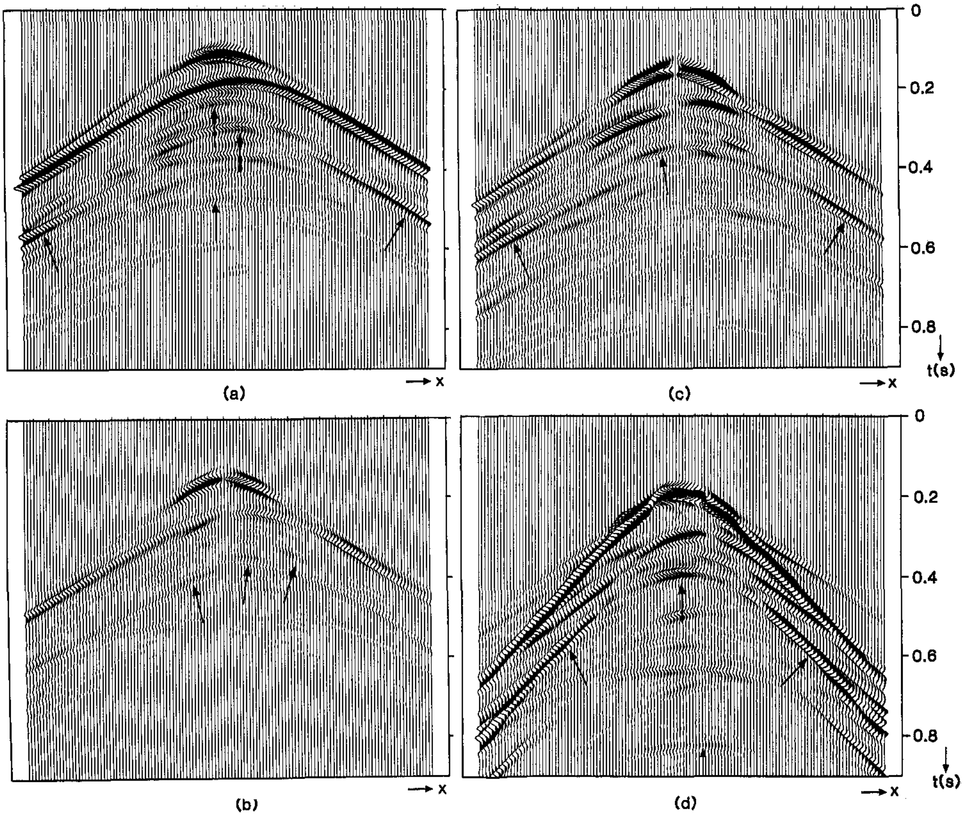

FIG. 13. Multicomponent shot record, after decomposition into one-way P- and S_y-wave responses. The source position is indicated by the arrow in Fig. 10. (a) True P–P data (see Fig. 9a); (b) true S_y–P data (see Fig. 9b); (c) true P–S_y data (see Fig. 9c); (d) true S_y–S_y data (see Fig. 9d). The arrows indicate surface-related multiple reflections and conversions.

According to (15), surface-related multiple elimination involves source signature deconvolution, i.e. removal of $s(\omega)$ from the data, according to (15a), and multiple prediction and subtraction, according to (15c).

Note that the multiple predictor

$$- \mathbf{X}_{\mathrm{fr}}(z_0) \sum_{m=1}^{\infty} (-\mathbf{R}_{\mathrm{fr}}^{-}(z_0)\mathbf{X}_{\mathrm{fr}}(z_0))^m$$

is fully determined by the free surface response matrix $\mathbf{X}_{\mathrm{fr}}(z_0)$ and the free surface reflection matrix $\mathbf{R}_{\mathrm{fr}}^{-}(z_0)$. Hence, no knowledge of the subsurface is required for surface-related multiple elimination. Only knowledge of the source signature $s(\omega)$ is required for the deconvolution. However, when the source signature is not known, it can be estimated by applying adaptive multiple elimination. This can be considered as a standard minimization problem: the multiple reflections are optimally removed

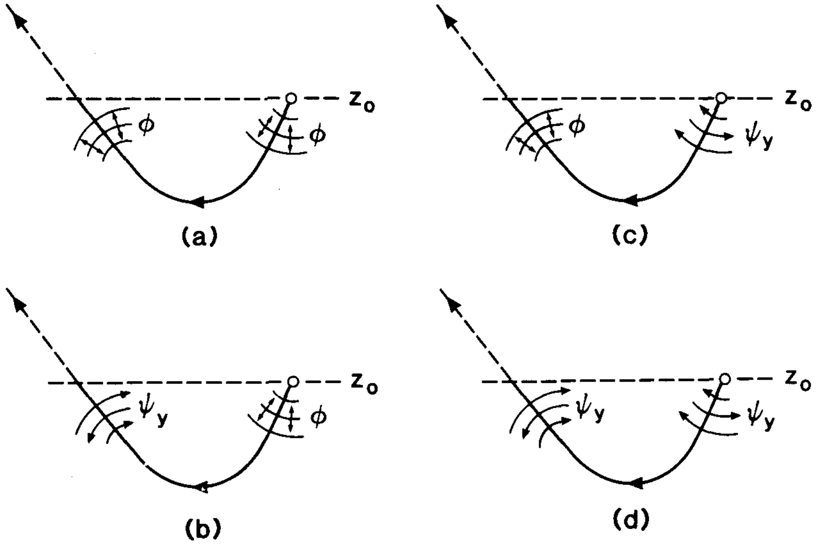

FIG. 14. 2D visualization of decomposed data at a reflection-free surface z_0 (after surface-related elastic multiple elimination).

(i.e. the energy in the broad-band data is minimized) when the correct source signature is used for the deconvolution. Hence, using an adaptive procedure, the source deconvolution and the multiple elimination are carried out simultaneously. For a further discussion on adaptive elimination of surface-related multiple reflections, see Verschuur *et al.* (1989). Note that the final result may be written as

$$\mathbf{X}(z_0) = \begin{pmatrix} \mathbf{X}_{\phi,\phi}(z_0) & \mathbf{X}_{\phi,\psi_x}(z_0) & \mathbf{X}_{\phi,\psi_y}(z_0) \\ \mathbf{X}_{\psi_x,\phi}(z_0) & \mathbf{X}_{\psi_x,\psi_x}(z_0) & \mathbf{X}_{\psi_x,\psi_y}(z_0) \\ \mathbf{X}_{\psi_y,\phi}(z_0) & \mathbf{X}_{\psi_y,\psi_x}(z_0) & \mathbf{X}_{\psi_y,\psi_y}(z_0) \end{pmatrix}. \tag{16}$$

Any of the sub-matrices simulates a (monochromatic) single-component one-way seismic survey at a reflection-free surface. In Fig. 14a the situation is shown for one element of matrix $\mathbf{X}_{\phi,\phi}(z_0)$. Similarly, in Figs 14b, c and d the situation is shown for the corresponding elements in matrices $\mathbf{X}_{\psi_y,\phi}(z_0)$, $\mathbf{X}_{\phi,\psi_y}(z_0)$ and $\mathbf{X}_{\psi_y,\psi_y}(z_0)$, respectively. We illustrate the elastic multiple elimination procedure with a 2D example. We consider the decomposed data of the example in the previous section. Using our adaptive procedure, the phase and amplitude of the source signature were estimated and the surface-related multiples were eliminated. One multicomponent shot record after adaptive multiple elimination is shown in Fig. 15. Note that this result clearly shows the primary one-way response (including minor internal multiple reflections and conversions) of the subsurface configuration of Fig. 10. This is confirmed by Fig. 16, which was obtained by forward modelling, assuming a reflection-free acquisition surface. Note that there are hardly any visible differences between Figs 15 and 16.

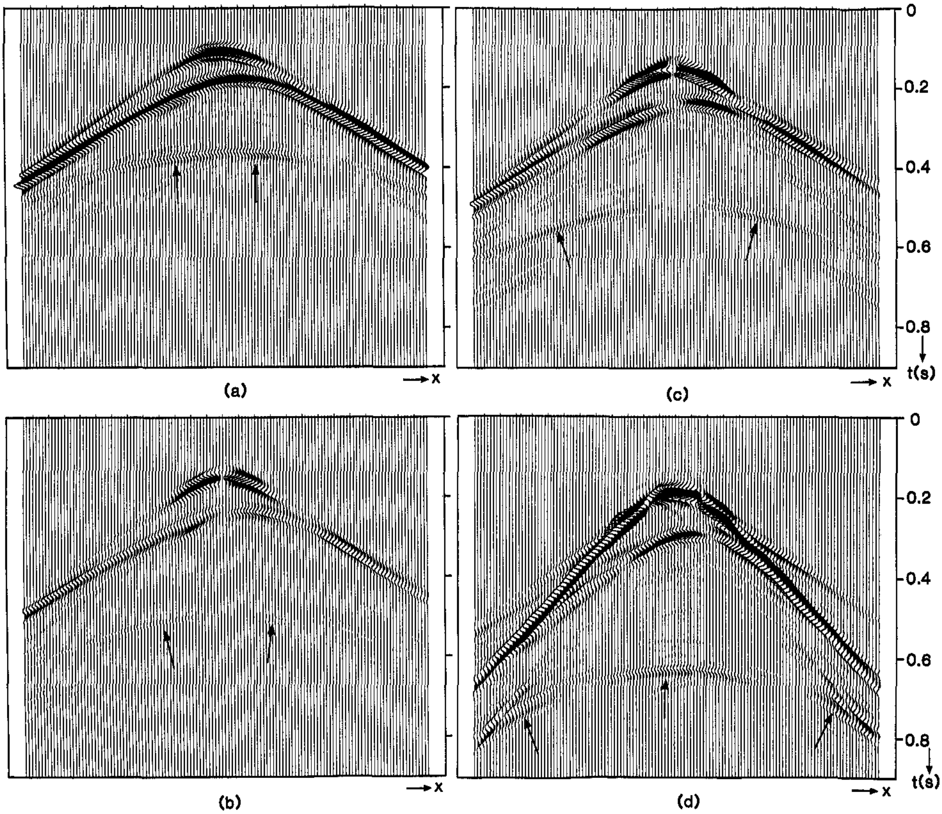

FIG. 15. Multicomponent shot record, after elastic multiple elimination. The source position is indicated by the arrow in Fig. 10. (a) True P–P data (see Fig. 14a); (b) true S_y–P data (see Fig. 14b); (c) true P–S_y data (see Fig. 14c); (d) true S_y–S_y data (see Fig. 14d). The arrows indicate the response of the target reflectors below $z_t = 450$ m.

CONCLUSIONS

Each data panel in a multicomponent seismic data set contains a mixture of P- and S-wave responses, including strong multiples and conversions related to the free surface (Figs 7 and 12). We have introduced a surface-related preprocessing procedure which consists of the following two steps (assuming the direct waves have been removed):

1. Decomposition of the multicomponent data set into P- and S-wave responses, in matrix notation described by (13a),

$$\mathbf{X}_{\mathrm{fr}}^{(s)}(z_0) = [\mathbf{C}(z_0)]^{-1}\mathbf{V}(z_0)[\mathbf{D}(z_0)]^{-1}. \tag{17}$$

In the resulting data set, the P- and S-wave responses are separated. However, the strong multiples and conversions related to the free surface are still present (Figs 9 and 13).

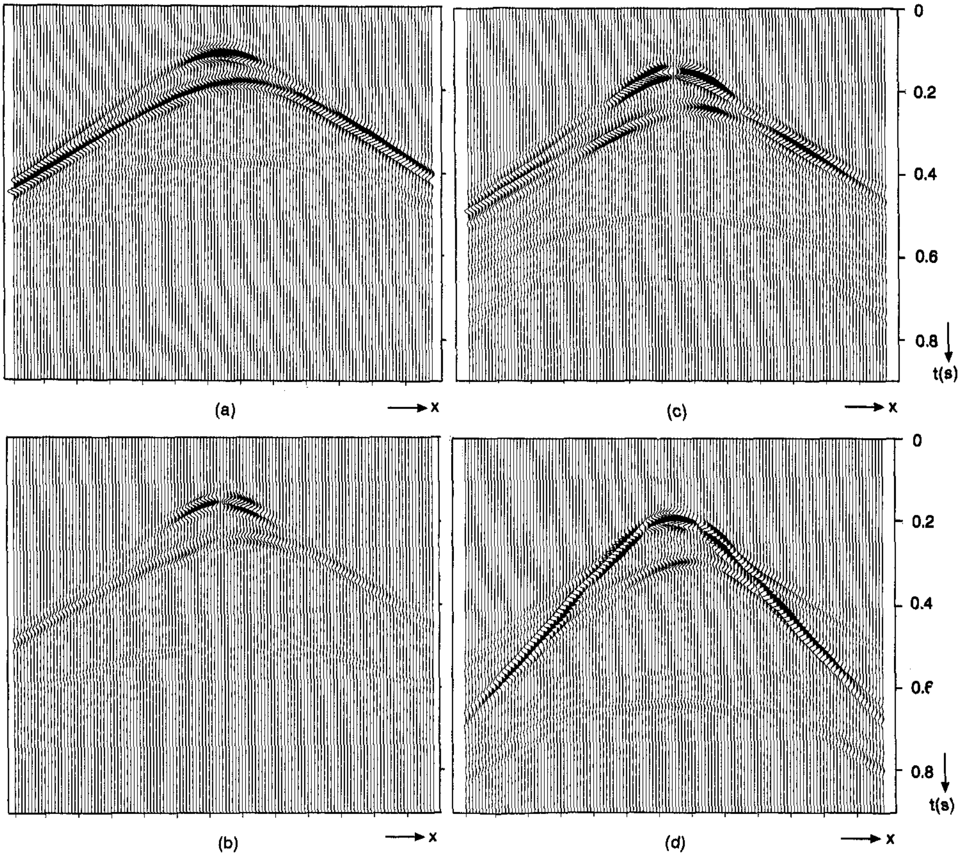

FIG. 16. Multicomponent shot record, obtained by forward modelling. The acquisition surface z_0 in Fig. 10 was assumed reflection-free. (a) True P–P data (see Fig. 14a); (b) true S_y–P data (see Fig. 14b); (c) true P–S_y data (see Fig. 14c); (d) true S_y–S_y data (see Fig. 14d).

2. Elimination of surface-related multiples and conversions, in matrix notation described by (15a) and (15c),

$$\mathbf{X}_{\mathrm{fr}}(z_0) = \frac{1}{s(\omega)}\,\mathbf{X}_{\mathrm{fr}}^{(s)}(z_0) \tag{18a}$$

and

$$\mathbf{X}(z_0) = \mathbf{X}_{\mathrm{fr}}(z_0)\left[\mathbf{I} + \sum_{m=1}^{\infty}\left(-\mathbf{R}_{\mathrm{fr}}^{-}(z_0)\mathbf{X}_{\mathrm{fr}}(z_0)\right)^m\right]. \tag{18b}$$

The source signature $s(\omega)$ in (18a) is obtained adaptively by minimizing the energy in $\mathbf{X}(z_0)$. In the resulting data set, the P- and S-wave responses are separated and the strong multiples and conversions related to the free surface have been removed (Figs 14 and 15). The remaining artefacts are related to internal multiples and conversions. In most practical situations these effects are significantly smaller than the surface-related multiples and conversions (compare Figs 12 and 15).

The procedure is valid for any inhomogeneous anisotropic subsurface with an inhomogeneous isotropic surface layer.

An interesting aspect of the procedure is that no knowledge of the subsurface is required.

The subsurface may have any degree of complexity. In the decomposition algorithm (17), the matrices $\mathbf{C}(z_0)$ and $\mathbf{D}(z_0)$ are fully determined by the medium parameters at the free surface z_0. Similarly, in the multiple elimination algorithm (18), the reflectivity matrix $\mathbf{R}_{\mathrm{fr}}^{-}(z_0)$ is also fully determined by the medium parameters at the free surface z_0. Hence, only the isotropic surface layer is assumed to be known.

Decomposition into primary P- and S-wave responses (steps 1 and 2) is proposed by Berkhout and Wapenaar (1988) as a preprocessing procedure, prior to elastic migration and inversion (Fig. 1).

Acknowledgements

We thank our colleague G. C. Haimé for generating the input data for the example. These investigations were supported by the Royal Dutch Academy of Sciences (C.P.A.W.), the Compagnie Générale de Géophysique (P.H.), the Dutch Science Foundation (D.J.V.) and the sponsors of the Delphi consortium.

Appendix A

Matrix/Vector Notation for Discretized Wavefields

We review Berkhout's matrix notation, generalized for 2D and 3D applications.

Consider a 2D wavefield, measured at a constant depth level as a function of lateral position and time, described by

$$p(x, z_0, t), \tag{A1a}$$

where

- p wavefield (for instance the acoustic pressure),
- x lateral coordinate of the receivers,
- z_0 depth level of the acquisition surface,
- t time.

After a Fourier transformation from time to frequency, this wavefield is described by

$$p(x, z_0, \omega), \tag{A1b}$$

where

p Fourier-transformed wavefield,
ω circular frequency.

In the following we only consider the frequency-domain representation, that is, we assume that monochromatic wavefields $p(x, z_0, \omega_i)$ are available for a range of ω_i values. All these monochromatic wavefields can be treated independently. If we consider one frequency component ω_i only, then the discretized version of the wavefield can be represented by a vector, according to

$$\mathbf{p}(z_0) = \begin{pmatrix} p(-K\,\Delta x, z_0, \omega_i) \\ \vdots \\ p(k\,\Delta x, z_0, \omega_i) \\ \vdots \\ p(K\,\Delta x, z_0, \omega_i) \end{pmatrix}, \tag{A1c}$$

where Δx is the distance between the receivers.

For the seismic situation this vector may represent the (monochromatic) data in one common shot record. Let us now write this vector symbolically as

$$\mathbf{p}(z_0) = \begin{array}{c} \begin{pmatrix} p_{-K} \\ \vdots \\ p_k \\ \vdots \\ p_K \end{pmatrix} \end{array} \begin{array}{c} \\ \\ \\ \downarrow \\ x_r \end{array}, \tag{A2a}$$

where x_r denotes that the different elements in this vector correspond to the different lateral positions of the receivers. With this notation we can write the (monochromatic) data $p(x_r, x_s, z_0, \omega_i)$ in a 2D seismic survey symbolically as a matrix, according to

$$\mathbf{P}(z_0) = \begin{array}{c} \rightarrow x_s \\ \begin{pmatrix} p_{-K,-M} & \cdots & p_{-K,m} & \cdots & p_{-K,M} \\ \vdots & & \vdots & & \vdots \\ p_{k,-M} & \cdots & p_{k,m} & \cdots & p_{k,M} \\ \vdots & & \vdots & & \vdots \\ p_{K,-M} & \cdots & p_{K,m} & \cdots & p_{K,M} \end{pmatrix} \end{array} \begin{array}{c} \\ \\ \\ \\ \downarrow \\ x_r \end{array}, \tag{A2b}$$

where x_s denotes the different lateral positions of the sources. Each element $p_{k,m}$ corresponds to a fixed lateral receiver coordinate $x_{r,k}$ and a fixed lateral source coordinate $x_{s,m}$. Each column (fixed x_s) in this data matrix represents one (monochromatic) common shot record; each row (fixed x_r) represents one common receiver record; the diagonal ($x_s = x_r$) represents zero-offset data and the anti-diagonal ($x_s = -x_r$) represents common midpoint data.

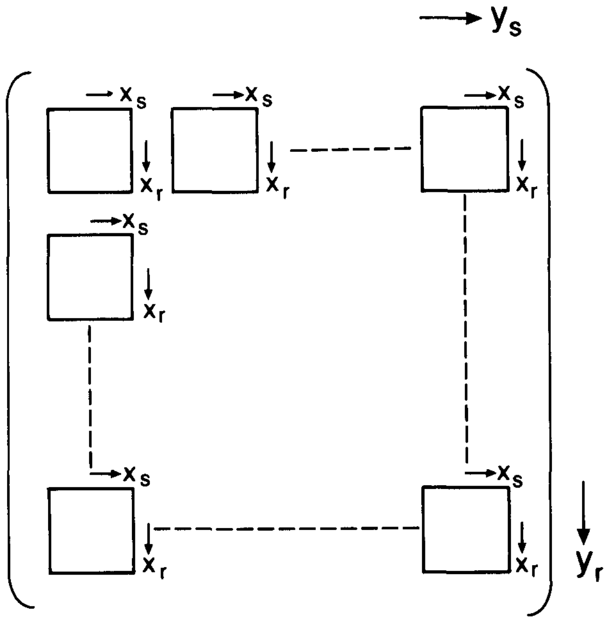

FIG. 17. Organization of the data matrix for a 3D seismic areal survey.

The (monochromatic) data $p(x_r, y_r, x_s, y_s, z_0, \omega_i)$ in a 3D seismic areal survey can also be represented by a matrix (Kinneging *et al.* 1989), according to

$$\begin{array}{cc} & \rightarrow y_s \\ \mathbf{P}(z_0) = \begin{pmatrix} \mathbf{P}_{-L,-N} & \cdots & \mathbf{P}_{-L,n} & \cdots & \mathbf{P}_{-L,N} \\ \vdots & & \vdots & & \vdots \\ \mathbf{P}_{l,-N} & \cdots & \mathbf{P}_{l,n} & \cdots & \mathbf{P}_{l,N} \\ \vdots & & \vdots & & \vdots \\ \mathbf{P}_{L,-N} & \cdots & \mathbf{P}_{L,n} & \cdots & \mathbf{P}_{L,N} \end{pmatrix}, & \begin{array}{c} \downarrow \\ y_r \end{array} \end{array} \tag{A2c}$$

where y_r denotes the different cross-line positions of the receivers and where y_s denotes the different cross-line positions of the sources. Each submatrix $\mathbf{P}_{l,n}$ corresponds to a fixed cross-line receiver coordinate $y_{r,l}$ and a fixed cross-line source coordinate $y_{s,n}$. The elements in the sub-matrix itself are defined as in (A2b) (see Fig. 17). Note that each column (fixed x_s, y_s) of the total matrix $\mathbf{P}(z_0)$ represents one (monochromatic) common shot record and each row (fixed x_r, y_r) represents one common receiver record. Throughout this paper a data matrix $\mathbf{P}(z_0)$ may represent either a 2D seismic survey, as in (A2b), or a 3D seismic areal survey, as in (A2c). Hence, a data vector $\mathbf{p}(z_0)$ (one column of $\mathbf{P}(z_0)$) may represent either a 2D or a 3D seismic shot record.

APPENDIX B

TWO-WAY AND ONE-WAY ELASTIC WAVE FIELDS

We shall derive the relationship between two-way elastic wavefields (in terms of the total particle velocity and traction) and one-way elastic wavefields (in terms of potentials for downgoing and upgoing P- and S-waves). For the moment, vectors denote continuous elastic wavefields, just as in the common literature on elastic wave theory. In a homogeneous isotropic source free region, the elastic wave equation for the particle velocity reads, in the space-frequency domain,

$$(\lambda + 2\mu)\nabla(\nabla \cdot \mathbf{v}) - \mu\nabla \times \nabla \times \mathbf{v} + \rho\omega^2\mathbf{v} = \mathbf{0}, \tag{B1}$$

(λ and μ are the Lamé coefficients). Define Lamé potentials ϕ and $\boldsymbol{\psi}$ for P- and S-waves, respectively, according to (Pilant 1979; Aki and Richards 1980),

$$\mathbf{v} = \frac{-1}{\mathrm{i}\omega\rho}(\nabla\phi + \nabla \times \boldsymbol{\psi});\ \nabla \cdot \boldsymbol{\psi} = 0. \tag{B2}$$

The factor $-(\mathrm{i}\omega\rho)^{-1}$ is generally omitted. The reason that we use this factor is because in the limiting case of an ideal fluid ($\mu = 0$) the Lamé potential ϕ represents the acoustic pressure. Substitution of (B2) into (B1) yields two independent equations for P- and S-waves,

$$\nabla^2\phi + \frac{\rho\omega^2}{\lambda + 2\mu}\phi = 0 \tag{B3a}$$

and

$$\nabla^2\boldsymbol{\psi} + \frac{\rho\omega^2}{\mu}\boldsymbol{\psi} = \mathbf{0}. \tag{B3b}$$

Let us now define the 2D spatial Fourier transform of a space- and frequency-dependent function according to

$$\tilde{A}(k_x, k_y, z, \omega) = \iint_{-\infty}^{+\infty} A(x, y, z, \omega)\exp\,[i(k_x x + k_y y)]\,\mathrm{d}x\,\mathrm{d}y \tag{B4a}$$

and its inverse as

$$A(x, y, z, \omega) = \left(\frac{1}{2\pi}\right)^2 \iint_{-\infty}^{+\infty} \tilde{A}(k_x, k_y, z, \omega)\exp\,[-\mathrm{i}(k_x x + k_y y)]\,\mathrm{d}k_x\,\mathrm{d}k_y \tag{B4b}$$

In the following, a tilde ($\sim$) above a symbol denotes the wavenumber-frequency domain (k_x, k_y, z, ω). In the wavenumber-frequency domain, (B2) reads

$$\tilde{\mathbf{v}} = \begin{pmatrix} \tilde{v}_x \\ \tilde{v}_y \\ \tilde{v}_z \end{pmatrix} = \frac{-1}{\mathrm{i}\omega\rho} \begin{pmatrix} -\mathrm{i}k_x\tilde{\phi} - \dfrac{\partial\tilde{\psi}_y}{\partial z} - \mathrm{i}k_y\tilde{\psi}_z \\ -\mathrm{i}k_y\tilde{\phi} + \dfrac{\partial\tilde{\psi}_x}{\partial z} + \mathrm{i}k_x\tilde{\psi}_z \\ \dfrac{\partial\tilde{\phi}}{\partial z} + \mathrm{i}k_y\tilde{\psi}_x - \mathrm{i}k_x\tilde{\psi}_y \end{pmatrix}, \tag{B5a}$$

with

$$-\mathrm{i}k_x\tilde{\psi}_x - \mathrm{i}k_y\tilde{\psi}_y + \frac{\partial\tilde{\psi}_z}{\partial z} = 0. \tag{B5b}$$

The z-derivatives in (B5) follow from (B3a) and (B3b) in the wavenumber-frequency domain:

$$\frac{\partial^2\tilde{\phi}}{\partial z^2} = -\left(\frac{\rho\omega^2}{\lambda + 2\mu} - k_x^2 - k_y^2\right)\tilde{\phi}, \tag{B6a}$$

or

$$\frac{\partial\tilde{\phi}^{\pm}}{\partial z} = \mp \mathrm{i}k_{z,\mathrm{p}}\tilde{\phi}^{\pm}, \tag{B6b}$$

with

$$k_{z,\mathrm{p}} = \sqrt{k_\mathrm{p}^2 - k_x^2 - k_y^2},\ k_\mathrm{p}^2 = \frac{\rho\omega^2}{\lambda + 2\mu}. \tag{B6c}$$

Similarly

$$\frac{\partial^2\tilde{\boldsymbol{\psi}}}{\partial z^2} = -\left(\frac{\rho\omega^2}{\mu} - k_x^2 - k_y^2\right)\tilde{\boldsymbol{\psi}}, \tag{B7a}$$

or

$$\frac{\partial\tilde{\boldsymbol{\psi}}^{\pm}}{\partial z} = \mp \mathrm{i}k_{z,\mathrm{s}}\tilde{\boldsymbol{\psi}}^{\pm}, \tag{B7b}$$

with

$$k_{z,\mathrm{s}} = \sqrt{k_\mathrm{s}^2 - k_x^2 - k_y^2},\ k_\mathrm{s}^2 = \frac{\rho\omega^2}{\mu}. \tag{B7c}$$

Define $\tilde{\phi}$ and $\tilde{\boldsymbol{\psi}}$ as the sum of downgoing and upgoing waves, according to

$$\tilde{\phi} = \tilde{\phi}^{+} + \tilde{\phi}^{-}, \tag{B8a}$$

and

$$\tilde{\boldsymbol{\psi}} = \tilde{\boldsymbol{\psi}}^{+} + \tilde{\boldsymbol{\psi}}^{-}. \tag{B8b}$$

Now (B5) may be rewritten as

$$\tilde{\mathbf{v}} = \tilde{\mathbf{L}}_1^{+}\tilde{\mathbf{p}}^{+} + \tilde{\mathbf{L}}_1^{-}\tilde{\mathbf{p}}^{-}, \tag{B9a}$$

where

$$\tilde{\mathbf{p}}^{\pm} = \begin{pmatrix} \tilde{\phi}^{\pm} \\ \tilde{\psi}_x^{\pm} \\ \tilde{\psi}_y^{\pm} \end{pmatrix} \tag{B9b}$$

and

$$\tilde{\mathbf{L}}_1^{\pm} = \frac{1}{\rho\omega}\begin{pmatrix} k_x & \mp\dfrac{k_x k_y}{k_{z,\mathrm{s}}} & \mp\dfrac{(k_\mathrm{s}^2 - k_x^2)}{k_{z,\mathrm{s}}} \\ k_y & \pm\dfrac{(k_\mathrm{s}^2 - k_y^2)}{k_{z,\mathrm{s}}} & \pm\dfrac{k_x k_y}{k_{z,\mathrm{s}}} \\ \pm k_{z,\mathrm{p}} & -k_y & k_x \end{pmatrix}. \tag{B9c}$$

Note that we eliminated $\tilde{\psi}_z$ from (B5a) and (B5b). If we make use of the stress-velocity relations in the wavenumber-frequency domain,

$$\tilde{\boldsymbol{\tau}} = \begin{pmatrix} \tilde{\tau}_x \\ \tilde{\tau}_y \\ \tilde{\tau}_z \end{pmatrix} = \frac{1}{\mathrm{i}\omega}\begin{pmatrix} \mu\left(\dfrac{\partial \tilde{v}_x}{\partial z} - \mathrm{i}k_x\tilde{v}_z\right) \\ \mu\left(\dfrac{\partial \tilde{v}_y}{\partial z} - \mathrm{i}k_y\tilde{v}_z\right) \\ \lambda\left(-\mathrm{i}k_x\tilde{v}_x - \mathrm{i}k_y\tilde{v}_y + \dfrac{\partial \tilde{v}_z}{\partial z}\right) + 2\mu\dfrac{\partial \tilde{v}_z}{\partial z} \end{pmatrix} \tag{B10}$$

where $\tilde{\boldsymbol{\tau}}$ is the traction vector, then we obtain, in analogy with (B9a),

$$\tilde{\boldsymbol{\tau}} = \tilde{\mathbf{L}}_2^{+}\tilde{\mathbf{p}}^{+} + \tilde{\mathbf{L}}_2^{-}\tilde{\mathbf{p}}^{-}, \tag{B11a}$$

where

$$\tilde{\mathbf{L}}_2^{\pm} = \frac{\mu}{\rho\omega^2}\begin{pmatrix} \mp 2k_x k_{z,\mathrm{p}} & 2k_x k_y & (k_\mathrm{s}^2 - 2k_x^2) \\ \mp 2k_y k_{z,\mathrm{p}} & -(k_\mathrm{s}^2 - 2k_y^2) & -2k_x k_y \\ -(k_\mathrm{s}^2 - 2k_x^2 - 2k_y^2) & \pm 2k_y k_{z,\mathrm{s}} & \mp 2k_x k_{z,\mathrm{s}} \end{pmatrix}. \tag{B11b}$$

Equations (B9) and (B11) can be combined into one equation, according to

$$\begin{pmatrix} \tilde{\mathbf{v}} \\ \tilde{\boldsymbol{\tau}} \end{pmatrix} = \begin{pmatrix} \tilde{\mathbf{L}}_1^+ & \tilde{\mathbf{L}}_1^- \\ \tilde{\mathbf{L}}_2^+ & \tilde{\mathbf{L}}_2^- \end{pmatrix} \begin{pmatrix} \tilde{\mathbf{p}}^+ \\ \tilde{\mathbf{p}}^- \end{pmatrix}. \tag{B12}$$

This equation describes, in the wavenumber-frequency domain, composition of the total elastic wavefield from downgoing and upgoing P- and S-wave potentials.

Decomposition of the total elastic wavefield into downgoing and upgoing P- and S-wave potentials is described by the inverse of equation (B12)

$$\begin{pmatrix} \tilde{\mathbf{p}}^+ \\ \tilde{\mathbf{p}}^- \end{pmatrix} = \begin{pmatrix} \tilde{\mathbf{M}}_1^+ & \tilde{\mathbf{M}}_2^+ \\ \tilde{\mathbf{M}}_1^- & \tilde{\mathbf{M}}_2^- \end{pmatrix} \begin{pmatrix} \tilde{\mathbf{v}} \\ \tilde{\boldsymbol{\tau}} \end{pmatrix}, \tag{B13a}$$

where

$$\tilde{\mathbf{M}}_1^\pm = \frac{\mu}{2\omega} \begin{pmatrix} 2k_x & 2k_y & \pm \dfrac{(k_s^2 - 2(k_x^2 + k_y^2))}{k_{z,\mathrm{p}}} \\ \mp \dfrac{k_x k_y}{k_{z,\mathrm{s}}} & \pm \dfrac{(k_{z,\mathrm{s}}^2 - k_y^2)}{k_{z,\mathrm{s}}} & -2k_y \\ \mp \dfrac{(k_{z,\mathrm{s}}^2 - k_x^2)}{k_{z,\mathrm{s}}} & \pm \dfrac{k_x k_y}{k_{z,\mathrm{s}}} & 2k_x \end{pmatrix} \tag{B13b}$$

and

$$\tilde{\mathbf{M}}_2^\pm = \frac{1}{2} \begin{pmatrix} \mp \dfrac{k_x}{k_{z,\mathrm{p}}} & \mp \dfrac{k_y}{k_{z,\mathrm{p}}} & -1 \\ 0 & -1 & \pm \dfrac{k_y}{k_{z,\mathrm{s}}} \\ 1 & 0 & \mp \dfrac{k_x}{k_{z,\mathrm{s}}} \end{pmatrix}. \tag{B13c}$$

Composition and decomposition formulae conformable to (B12) and (B13) have been used by many authors. An outline is given by Ursin (1983). It should be noted, however, that we made an important modification with respect to the definition of the operators. Generally, the composition and decomposition operators contain terms such as (in our notation) $k_x/\sqrt{(k_x^2 + k_y^2)}$ and $k_y/\sqrt{(k_x^2 + k_y^2)}$. Note that these terms are discontinuous for $k_x = k_y = 0$, i.e. for vertical wave propagation. Transforming these expressions back to the space domain causes considerable artefacts. This problem is directly related to the choice of S-wave separation. Generally S-waves are sub-divided into SV-waves (polarization in the vertical plane through the wave vector and the z-axis) and SH-waves (horizontal polarization). Note that any vertically propagating S-wave can be classified as either an SV-wave or an SH-wave, hence, the decomposition problem is not unique. We avoided these problems by sub-dividing S-waves into S_x-waves (polarization in the plane perpendicular to the x-axis) and S_y-waves (polarization in the plane perpendicular to the y-axis). In our formulation, these wave types are represented by the S-wave potentials ψ_x and ψ_y, respectively.

Let us now derive the composition and decomposition formulas in the space-frequency domain. First we consider the decomposition algorithm (B13), which can be rewritten as

$$\tilde{p}_i^{\pm}(k_x, k_y, z, \omega) = \sum_{j=1}^{3} [\tilde{M}_{1,ij}^{\pm}(k_x, k_y, z, \omega)\tilde{v}_j(k_x, k_y, z, \omega) + \tilde{M}_{2,ij}^{\pm}(k_x, k_y, z, \omega)\tilde{\tau}_j(k_x, k_y, z, \omega)]. \tag{B14}$$

Here $\tilde{p}_i^{\pm}$ for $i = 1, 2, 3$ represents $\tilde{\phi}^{\pm}$, $\tilde{\psi}_x^{\pm}$ and $\tilde{\psi}_y^{\pm}$, respectively, see also (B9b). $\tilde{v}_j$ for $j = 1, 2, 3$ represents $\tilde{v}_x$, $\tilde{v}_y$ and $\tilde{v}_z$, respectively, see also (B5a). $\tilde{\tau}_j$ for $j = 1, 2, 3$ represents $\tilde{\tau}_x$, $\tilde{\tau}_y$ and $\tilde{\tau}_z$, respectively, see also (B10). Finally, $\tilde{M}_{1,ij}^{\pm}$ and $\tilde{M}_{2,ij}^{\pm}$ for $i = 1, 2, 3$ and $j = 1, 2, 3$ represents the elements of matrices $\tilde{\mathbf{M}}_1^{\pm}$ and $\tilde{\mathbf{M}}_2^{\pm}$, respectively, as defined by (B13b) and (B13c). Multiplications in the wavenumber domain correspond to convolutions in the space domain, hence

$$p_i^{\pm}(x, y, z, \omega) = \sum_{j=1}^{3} \iint_{-\infty}^{+\infty} M_{1,ij}^{\pm}(x, y, x', y', z, \omega) v_j(x', y', z, \omega)\, dx'\, dy' + \sum_{j=1}^{3} \iint_{-\infty}^{+\infty} M_{2,ij}^{\pm}(x, y, x', y', z, \omega) \tau_j(x', y', z, \omega)\, dx'\, dy', \tag{B15a}$$

with

$$M_{\alpha,ij}^{\pm}(x, y, x', y', z, \omega) = M_{\alpha,ij}^{\pm}(x - x', y - y', z, \omega), \tag{B15b}$$

for $\alpha = 1, 2$, where $M_{\alpha,ij}^{\pm}(x, y, z, \omega)$ is obtained by applying a band-limited version of the inverse Fourier transform (B4b) to the matrix elements $\tilde{M}_{\alpha,ij}^{\pm}(k_x, k_y, z, \omega)$.

From here onwards we adopt the matrix/vector notation of Appendix A. In this notation, the discretized version of (B15a) reads

$$\mathbf{p}_i^{\pm}(z) = \sum_{j=1}^{3} [\mathbf{M}_{1,ij}^{\pm}(z)\mathbf{v}_j(z) + \mathbf{M}_{2,ij}^{\pm}(z)\boldsymbol{\tau}_j(z)]. \tag{B16}$$

Here the vectors $\mathbf{p}_i^{\pm}(z)$, $\mathbf{v}_j(z)$ and $\boldsymbol{\tau}_j(z)$ contain the discretized scalar wavefields $p_i^{\pm}(x, y, z, \omega)$, $v_j(x, y, z, \omega)$ and $\tau_j(x, y, z, \omega)$. The matrices $\mathbf{M}_{1,ij}^{\pm}(z)$ and $\mathbf{M}_{2,ij}^{\pm}(z)$ contain the discretized operators $M_{1,ij}^{\pm}(x, y, x', y', z, \omega)\, \Delta x\, \Delta y$ and $M_{2,ij}^{\pm}(x, y, x', y', z, \omega)\, \Delta x\, \Delta y$ (Δx and Δy are the discretization intervals). The format of these operator matrices is the same as the format of the data matrix $\mathbf{P}(z_0)$ in (A2c), which contains the monochromatic data $p(x_r, y_r, x_s, y_s, z_0, \omega)$. Because of the special character of the operators (see (B15b)), operator matrices $\mathbf{M}_{1,ij}^{\pm}(z)$ and $\mathbf{M}_{2,ij}^{\pm}(z)$ are Toeplitz matrices. Note that (B16) may also be written as

$$\begin{pmatrix} \mathbf{p}^{+}(z) \\ \mathbf{p}^{-}(z) \end{pmatrix} = \begin{pmatrix} \mathbf{M}_1^{+}(z) & \mathbf{M}_2^{+}(z) \\ \mathbf{M}_1^{-}(z) & \mathbf{M}_2^{-}(z) \end{pmatrix} \begin{pmatrix} \mathbf{v}(z) \\ \boldsymbol{\tau}(z) \end{pmatrix}, \tag{B17a}$$

where

$$\mathbf{p}^{\pm}(z) = \begin{pmatrix} \mathbf{p}_1^{\pm}(z) \\ \mathbf{p}_2^{\pm}(z) \\ \mathbf{p}_3^{\pm}(z) \end{pmatrix} = \begin{pmatrix} \boldsymbol{\phi}^{\pm}(z) \\ \boldsymbol{\psi}_x^{\pm}(z) \\ \boldsymbol{\psi}_y^{\pm}(z) \end{pmatrix}, \tag{B17b}$$

$$\mathbf{v}(z) = \begin{pmatrix} \mathbf{v}_x(z) \\ \mathbf{v}_y(z) \\ \mathbf{v}_z(z) \end{pmatrix}, \tag{B17c}$$

$$\boldsymbol{\tau}(z) = \begin{pmatrix} \boldsymbol{\tau}_x(z) \\ \boldsymbol{\tau}_y(z) \\ \boldsymbol{\tau}_z(z) \end{pmatrix}, \tag{B17d}$$

and

$$\mathbf{M}_\alpha^{\pm}(z) = \begin{pmatrix} \mathbf{M}_{\alpha,11}^{\pm}(z) & \mathbf{M}_{\alpha,12}^{\pm}(z) & \mathbf{M}_{\alpha,13}^{\pm}(z) \\ \mathbf{M}_{\alpha,21}^{\pm}(z) & \mathbf{M}_{\alpha,22}^{\pm}(z) & \mathbf{M}_{\alpha,23}^{\pm}(z) \\ \mathbf{M}_{\alpha,31}^{\pm}(z) & \mathbf{M}_{\alpha,32}^{\pm}(z) & \mathbf{M}_{\alpha,33}^{\pm}(z) \end{pmatrix}, \tag{B17e}$$

for $\alpha = 1, 2$. In a similar way we can derive the space-frequency domain representation of the composition algorithm (B12), yielding

$$\begin{pmatrix} \mathbf{v}(z) \\ \boldsymbol{\tau}(z) \end{pmatrix} = \begin{pmatrix} \mathbf{L}_1^{+}(z) & \mathbf{L}_1^{-}(z) \\ \mathbf{L}_2^{+}(z) & \mathbf{L}_2^{-}(z) \end{pmatrix} \begin{pmatrix} \mathbf{p}^{+}(z) \\ \mathbf{p}^{-}(z) \end{pmatrix}, \tag{B18a}$$

where

$$\mathbf{L}_\alpha^{\pm}(z) = \begin{pmatrix} \mathbf{L}_{\alpha,11}^{\pm}(z) & \mathbf{L}_{\alpha,12}^{\pm}(z) & \mathbf{L}_{\alpha,13}^{\pm}(z) \\ \mathbf{L}_{\alpha,21}^{\pm}(z) & \mathbf{L}_{\alpha,22}^{\pm}(z) & \mathbf{L}_{\alpha,23}^{\pm}(z) \\ \mathbf{L}_{\alpha,31}^{\pm}(z) & \mathbf{L}_{\alpha,32}^{\pm}(z) & \mathbf{L}_{\alpha,33}^{\pm}(z) \end{pmatrix}, \tag{B18b}$$

for $\alpha = 1, 2$, where submatrices $\mathbf{L}_{\alpha,ij}^{\pm}(z)$ contain the discretized operators

$$L_{\alpha,ij}^{\pm}(x, y, x', y', z, \omega) = L_{\alpha,ij}^{\pm}(x - x', y - y', z, \omega) \tag{B18c}$$

for $\alpha = 1, 2$, $L_{\alpha,ij}^{\pm}(x, y, z, \omega)$ being the inverse Fourier transform of $\mathbf{L}_{\alpha,ij}^{\pm}(k_x, k_y, z, \omega)$.

Note that the decomposition operators in (B17a) are related to the composition operators in (B18a) according to

$$\mathbf{M}_1^{\pm} = (\mathbf{L}_1^{\pm} - \mathbf{L}_1^{\mp}(\mathbf{L}_2^{\mp})^{-1}\mathbf{L}_2^{\pm})^{-1} \tag{B19a}$$

and

$$\mathbf{M}_2^{\pm} = (\mathbf{L}_2^{\pm} - \mathbf{L}_2^{\mp}(\mathbf{L}_1^{\mp})^{-1}\mathbf{L}_1^{\pm})^{-1}. \tag{B19b}$$

Also note that (B18a) can be used elegantly to derive the reflection matrix $\mathbf{R}_{\mathrm{fr}}^{-}(z_0)$ for a free surface at $z = z_0$. For the situation depicted in Fig. 18 we write

$$\mathbf{p}^{+}(z_0) = \mathbf{R}_{\mathrm{fr}}^{-}(z_0)\mathbf{p}^{-}(z_0). \tag{B20a}$$

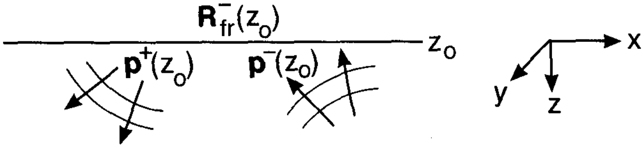

FIG. 18. Reflection at the free surface of an elastic half-space.

Substituting this expression into (B18a), using the free surface property $\boldsymbol{\tau}(z_0) = \mathbf{0}$, yields

$$\mathbf{0} = [\mathbf{L}_2^+(z_0)\mathbf{R}_{fr}^-(z_0) + \mathbf{L}_2^-(z_0)]\mathbf{p}^-(z_0), \tag{B20b}$$

or, since this expression should hold for any upgoing wavefield $\mathbf{p}^-(z_0)$,

$$\mathbf{R}_{fr}^-(z_0) = -[\mathbf{L}_2^+(z_0)]^{-1}\mathbf{L}_2^-(z_0). \tag{B20c}$$

So far we have considered the homogeneous situation. Variations of the medium parameters can be accounted for by designing the operators $L^{\pm}_{\alpha,\,ij}(x, y, x', y', z, \omega)$ and $M^{\pm}_{\alpha,\,ij}(x, y, x', y', z, \omega)$ for $\alpha = 1, 2$ in accordance with the local medium parameters at (x, y, z). In this case (B15b) and (B18c) are no longer valid, so matrices $\mathbf{L}_\alpha^{\pm}$ and $\mathbf{M}_\alpha^{\pm}$ lose their simple Toeplitz structure.

Blacquière *et al.* (1989) discuss the design of optimized operators $F^{\pm}(x, y, x', y', z, \omega)$ for 3D inverse wavefield extrapolation in inhomogeneous media. Their approach can be easily adapted for the design of optimized operators $L^{\pm}_{\alpha,\,ij}(x, y, x', y', z, \omega)$ and $M^{\pm}_{\alpha,\,ij}(x, y, x', y', z, \omega)$ for 3D elastic wavefield decomposition in inhomogeneous media. A further discussion of operator optimization is beyond the scope of this paper.

REFERENCES

AKI, K. and RICHARDS, P.G. 1980. *Quantitative Seismology*. W.H. Freeman and Co.

BERESFORD-SMITH, G. and RANGO, R. 1989. Suppression of ground roll by windowing in two domains. *First Break* **7**, 55–63.

BERKHOUT, A.J. 1982. *Seismic Migration: Imaging of acoustic energy by wave field extrapolation. A. Theoretical aspects.* Elsevier Science Publishing Co.

BERKHOUT, A.J. and WAPENAAR, C.P.A. 1988. Delft philosophy on inversion of elastic data. 58th SEG meeting, Anaheim, U.S.A., Expanded Abstracts, 831–833.

BLACQUIÈRE, G., DEBEYE, H.W.J., WAPENAAR, C.P.A. and BERKHOUT, A.J. 1989. Three-dimensional table-driven migration. *Geophysical Prospecting* **37**, 925–958.

CLIET, C. and DUBESSET, M. 1987. Three-component recordings: Interest for land seismic source study. *Geophysics* **52**, 1048–1059.

DANKBAAR, J.W.M. 1985. Separation of P- and S-waves. *Geophysical Prospecting* **33**, 970–986.

HAIMÉ, G.C. 1987. Full elastic inverse wave field extrapolation through an inhomogeneous medium. M.Sc. thesis, Delft University of Technology.

KELLY, K.R., WARD, R.W., TREITEL, S. and ALFORD, R.M. 1976. Synthetic seismograms: a finite difference approach. *Geophysics* **41**, 2–27.

KENNETT, B.L.N. 1979. The suppression of surface multiples on seismic records. *Geophysical Prospecting* **27**, 584–600.

KENNETT, B.L.N. 1984. An operator approach to forward modeling, data processing and migration. *Geophysical Prospecting* **32**, 1074–1090.

KINNEGING, N.A., BUDEJICKY, V., WAPENAAR, C.P.A. and BERKHOUT, A.J. 1989. Efficient 2D and 3D shot record redatuming. *Geophysical Prospecting* **37**, 493–530.

PILANT, W.L. 1979. *Elastic Waves in the Earth.* Elsevier Science Publishing Co.

URSIN, B. 1983. Review of elastic and electromagnetic wave propagation in horizontally layered media. *Geophysics* **48**, 1063–1081.

VERSCHUUR, D.J., BERKHOUT, A.J. and WAPENAAR, C.P.A. 1989. Wavelet estimation by pre-stack multiple elimination. 59th SEG meeting, Dallas, U.S.A., Expanded Abstracts, 1129–1132.

WAPENAAR, C.P.A. and BERKHOUT, A.J. 1989. *Elastic Wave Field Extrapolation: Redatuming of single- and multi-component seismic data.* Elsevier Science Publishing Co.

WAPENAAR, C.P.A. and HAIMÉ, G.C. 1990. Elastic extrapolation of primary seismic P- and S-waves. *Geophysical Prospecting* **38**, 23–60.